INVESTIGATION AND IMPLEMENTATION OF SOLAR PV BASED FORWARD MICROCONVERTER

[1]M.Premkumar, [2]T.R.Sumithira

[1]Assistant Professor, Department of EEE, GMR Institute of Technology, Rajam, AP, India

[2]Assistant Professor, Department of EEE, Government College of Engineering, Salem, TN, India

[1]mprem.me@gmail.com, [2]sumithra.trs@gmail.com

[3]R.Sowmya

[3]Research Scholar, National Institute of Technology, Tiruchirapalli, TN, India

[3]sowmyanitt@gmail.com

Abstract *- Nowadays, many alternate solutions are there to overcome the traditional power grid blackout and it results in an increase in research on the various field. The solar photovoltaic (PV) powered microconverter is the way to increase the performance nowadays. The analysis and implementation of such converter are discussed in this paper. The various Maximum Power Point Tracking (MPPT) techniques are applied to the DC-DC converter to extract the maximum and optimal power from the PV panel. The main objective of this paper is to design a closed-loop DC-DC Converter to boost the voltage from the PV cell and supplied to the load with high efficiency. The converter selected in this paper is single ended primary inductor converter (SEPIC) converter and it offers low voltage stress on the switch and simple design. The switching loss is less due to single switch with low-frequency switching. The gating and commutation components are less and therefore the conduction loss is also less. The microconverter is analyzed and simulated for closed-loop control and it concludes suitability of the converter for solar PV application. Finally, the prototype is developed for 80W and the results are verified experimentally.*

Keywords *– Closed-loop, Microconverter, SEPIC, Switching loss, Voltage stress.*

I. INTRODUCTION

In PV based system, microconverter is the rapidly growing technology in future for domestic application. The microconverters are used to boost up the voltage from the PV panel and it is particularly designed to extract the highest power ranges from 80W – 250W [1]-[2]. The various advantages like localized MPPT, robustness and easy installation makes it suitable for domestic application when compared to other converter techniques. Comparatively, the string inverters offer the highest efficiency in energy capturing. But, if any of the cell/panel in series are shaded, the energy capturing will be reduced [3]. The shadowing effect on the PV panel is shown in Fig. 1.

Fig. 1. Effect on PV Panel due to Shadowing

Due to localized MPPT, microconverters adds extra cost per PV module but the performance of the converters is increased by 2-10%. The microconverter recovers more losses than the other converter such as loss due to shading, panel mismatch loss and MPPT loss. Finally, the microconverter loses its converter efficiency but offer more energy capturing [4]. The output of the converters is connected in parallel and routed to the common point. There is no series/parallel DC connection to keep the DC voltage at relatively lower level. The key parameter comparison is listed in Table 1 to find the optimal application of the various inverter [6].

Table 1. Comparison of the Inverter Key Parameters

	Power	Voltage	Maximum Efficiency	Cost	Cost/Watt
Microinverter	< 250W	20V – 100 V	98%	Low	High
String Inverter	< 25kW	100V – 1100V	97%	Medium	Medium
Central Inverter	> 25kW	400V – 1600V	97.5%	Very High	Low

The microinverters are reviewed in [5] and it is classified as single and multi-stage topology. In single-stage topology, the

voltage, current and power modulation are done in the single stage and it has less complexity in design and simple to control. It fails to give high efficiency during wide operating region. Since the power optimization is done at each stage of multi-stage topology, the efficiency of the converter is good, but the requirement of more component and control complexity makes this topology complex.

The localized MPPT is achieved by the individual converter with each of the solar PV panels. Many DC-DC converters such as buck, boost, buck-boost, flyback, SEPIC, CUK and much more can increase/decrease the DC voltage level as per the requirement by the load/inverter [7]-[8]. Out of which, this paper deals with SEPIC converter and it is normally operated at the high switching frequency. But the high-frequency switching increases the diode reverse recovery current, electromagnetic interference (EMI) noise, and switching loss. Compared to the buck-boost converter, power handling capacity of MOSFET is less in SEPIC at the same power level. So, the reverse recovery loss is less in SEPIC than boost/buck-boost converter. The inductor leakage energy will be taken care of by the decoupling circuit. So, the dissipative circuits are not needed additionally which reduces the power loss and improves the efficiency of the converter [9]-[10].

The closed-loop control will improve the robustness and reliability of the dc-dc converter than the open loop control. In most of the literature, dc-dc converter fault diagnosis is focused on the open loop control. Due to the influence of closed-loop feedback, the relation between the various variables and operating characteristics of the converter is more complex than open loop. The design part of SEPIC converter controller is complex even the performance of the converter is good. In [11], it is discussed that SEPIC converter will be unstable due to 4th order non-minimum phase and poor design of the controller. This paper utilizes loop shaping technique to design the closed loop system feedback loop for the SEPIC converter.

The organization of the paper is as follows: Section 2 discusses the basic circuit topology and operating mode of the converter. The modelling of the converter, operation and design parameters are presented in section 3. Section 4 discusses the simulation and hardware results to show the performance of the SEPIC converter in closed-loop control. Finally, section 5 concludes the paper.

II. Basic Converter Topology

The SEPIC converter power stages are as follows. The solar PV module energizes the dc-dc converter with 36V input supply. The converter boosts up the voltage with the help MOSFET switch, boost inductor and energy storage element. The SEPIC converter is operated in two modes depends on the flow of load current. The modes are nothing but Continuous Conduction Mode (CCM) or Discontinuous Conduction Mode (DCM). For ease of understanding and with the assumption of continuous load current, the converter in this paper is discussed only for the CCM.

2.1 Operating Modes of the SEPIC Converter

The assumption for modelling and design the converter is discussed in a subsequent section of this paper. If the converter is operated at CCM, the converter has low inductor ripple current and if the converter is operated at DCM, the converter has high inductor ripple current. Since the input current continuous and low inductor ripple current, the converter is operated at CCM. In CCM, the voltage gain of the converter is independent of the load type. Whereas, in DCM, a gain of the converter is depending on the type of the load, boost inductor and switching frequency. The efficiency of the converter with CCM is higher than DCM. But the converter at CCM supplies switching loss due to the reverse recovery of the diode. The input current is pulsating even the size of the inductor is less in CCM. The converter may be operated in both the modes but in this paper, the converter is tested with CCM [12]-[15].

2.2 Proposed Converter Block Diagram

As discussed earlier, to improve the robustness and reliability of the converter, closed-loop control is adopted in place of open loop control. The block diagram for the closed-loop control is shown in Fig. 2.

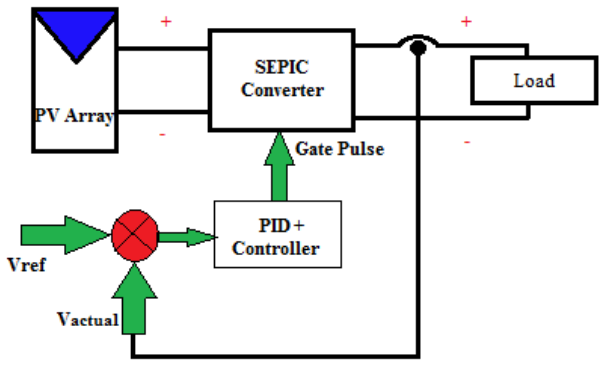

Fig. 2. Block Diagram for the Closed Loop Control

The load voltage is sensed by the voltage sensor and taken as a feedback to control the operation of the converter. The converter is designed with current mode PWM control IC UC2843. The converter is operated at 20-100V input with

100kHz switching frequency with output voltage ripple less than 5% of the output voltage. The feedback loop is designed with PID controller and it is tuned by loop shaping technique for better transient and steady response of the converter. The rise time of the converter is reduced by P-controlled and steady-state error will be reduced by the I-controller. So, the PI controller is selected for the design and the same is discussed in this paper. The required output voltage is obtained by the changing reference voltage of the converter.

III. Modelling And Operating Of The Sepic Converter

3.1 Modelling of SEPIC Converter

The main function of the solar PV powered SEPIC converter is as follows:

1) Regulates the DC output voltage
2) Tracks the maximum power by employing MPP
3) Boost the output voltage of the solar PV as per the required voltage

Due to the buck-boost characteristics without inverting the voltage, SEPIC converter is considered in this paper. The converter is modelled as per the Eqs. 1-11 and the converter is operated in CCM [16]-[17]. The output voltage of the converter is presented in Eq. 1.

$$\mathrm{V}_{out} = V_{in} * \frac{\mathrm{D}}{1-\mathrm{D}} \tag{1}$$

where duty cycle of the converter is represented as D and it is represented in Eq. 2.

$$\mathrm{D} = \frac{\mathrm{V}_{out} + \mathrm{V}_d}{\mathrm{V}_{out} + \mathrm{V}_d + V_{in}} \tag{2}$$

where the diode voltage drop is represented as $\mathrm{V_d}$ and the maximum duty cycle of the converter is given in Eq. 3.

$$\mathrm{D_{max}} = \frac{\mathrm{V}_{out} + \mathrm{V}_d}{\mathrm{V}_{out} + \mathrm{V}_d + V_{in}(\mathrm{min})} \tag{3}$$

By approximating ripple current to be 30% of the input current, the value of the inductance is calculated at minimum input voltage. The inductor ripple current ($\Delta \mathrm{I}_L$) flows through the inductors and it is represented in Eq. 4.

$$\Delta \mathrm{I}_L = \mathrm{I}_{in} * 40\% = \mathrm{I}_{out} * \frac{\mathrm{V}_{out}}{V_{in}(\mathrm{min})} * \ 40\% \tag{4}$$

The value of the inductor is calculated as per Eq. 5.

$$\mathrm{L_1} = \mathrm{L_2} = \mathrm{L} = \frac{\mathrm{V_{in}(min)}}{\Delta \mathrm{I_L} * \mathrm{F_s}} * \mathrm{D_{max}} \tag{5}$$

The maximum value of the current through the inductor which guarantees the inductor saturation is given in Eq. 6.

$$\Delta \mathrm{I_{L1}(peak)} = \mathrm{I_{out}} * \frac{\mathrm{V_{out}} + \mathrm{V_d}}{\mathrm{V_{in}(min)}} * \left(\frac{1+30\%}{2}\right) \tag{6}$$

$$\Delta \mathrm{I_{L2}(peak)} = \mathrm{I_{out}} * \left(\frac{1+30\%}{2}\right) \tag{7}$$

The value of the coupling capacitor is depending on root-mean-square (RMS) value of the current and it is given in Eq. 8.

$$I_{C_s}(rms) = I_{out} * \sqrt{\frac{V_{out} + V_d}{V_{in}(min)}} \tag{8}$$

The coupling capacitor is selected for large RMS current and it allows the converter to operate at low power application. The size of the capacitor is relatively small. The coupling capacitor voltage should be more than the input voltage. For this purpose, electrolytic capacitors are more suitable. The change in voltage across the coupling capacitor is represented in Eq. 9.

$$\Delta \mathrm{V_{C_s}} = \frac{\mathrm{I_{out}} * \mathrm{D_{max}}}{\mathrm{C_s} * \mathrm{F_s}} \tag{9}$$

The value of the coupling capacitor is calculated as per the Eq. 10.

$$\mathrm{C_s} = \frac{\mathrm{D}}{\mathrm{R} * \frac{\Delta \mathrm{V_{C_s}}}{V_{out}} * \mathrm{F_s}} \tag{10}$$

When the switch Q1 is turned on, the output capacitor supplies the current to the load and the inductor started to charge. The output capacitor must withstand high RMS current because the capacitor subjected to high ripple current. The selection of the capacitor should meet the requirements such as the equivalent series resistor (ESR) and RMS current. The value of the capacitor is calculated as per Eq. 11.

$$\mathrm{C_O} \geq \frac{\mathrm{I_{out}} * \mathrm{D_{max}}}{\mathrm{V_{ripple}} * \mathrm{F_s}} \tag{11}$$

where the switching frequency is represented as F_s; the ripple current of the inductor L_1 and L_2 is represented as ΔI_{L1} and ΔI_{L2} respectively. The output represented as V_{out} and input voltage as V_{in}. The load resistance is represented as R. The solar PV panel specification is listed in Table 2 and SEPIC converter specification is listed in Table 3.

Table 2. Specification of the PV Panel

Parameters	Ratings
Rated Power (Pmax)	80W
Voltage at Pmax (Vmpp)	26V
Current at Pmax (Impp)	3.7A
Short circuit current (Isc)	4.8A
Open circuit voltage (Voc)	36V

Table 3. Specification of the SEPIC Converter

Parameters	Ratings
Input voltage range V_{in}	20-100V
Switching frequency F_s	100kHz
Output voltage V_{out}	300V
Rated output power P_{max}	80W
Input inductor L_1 and L_2	2.4mH
Coupling capacitor C_S	47uF
Output capacitor C_O	10uF

3.2. Operation of the SEPIC Converter

The simple circuit of the SEPIC converter is shown in Fig. 3. The converter consists of boost inductors, output capacitor, and coupling capacitor. The coupling capacitor is charged to the input voltage at the initial stage.

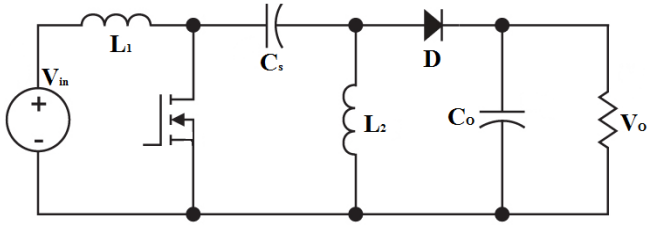

Fig. 3. Proposed SEPIC Converter

As discussed earlier, CCM mode is selected for the converter operation when the current flows through L_1 is not equal to zero. The voltage across the coupling capacitor is equal to the input voltage during steady state because the DC current is blocked by the capacitor so the average current is zero and it makes L_2 as the source for supplying the load current. The inductors are wound on the same core so the voltage across the inductor is equal and opposite i.e. V_{L1}=-V_{L2}. The effect due to mutual inductance is zero because the inductor voltage is equal. So, the ripple current through the inductors is equal. The load current is equal to the current through the inductor L_2 and it is not depending on the input voltage. Eq. 12 gives the input voltage.

$$V_{in} = V_{L_1} + V_{L_2} + V_{C_S} \tag{12}$$

When Q_1 is turned off, the output voltage and the voltage across L_2 is equal because the input capacitor is charged to the input voltage. The voltage across the switch is equal to $V_{in}+V_{out}$. Fig. 4 shows the overall operation of the converter when Q_1 is turned OFF.

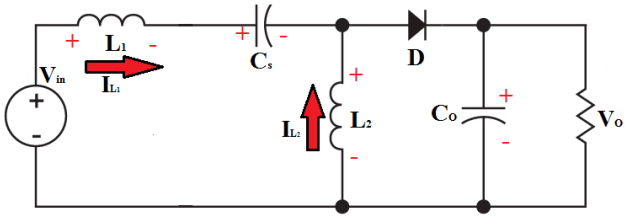

Fig. 4. Current Flow when Q_1 in OFF State

When Q1 is turned ON, the coupling capacitor is charged to the input voltage. The voltage across L_2 is equal to the input voltage and opposite i.e. $-V_{in}$. The current flow is shown in Fig. 5. During this mode, the stored energy in L_1 due to the input voltage and in L_2, due to the coupling capacitor C_S. The diode average current is represented in Eq. 13.

$$I_{D_1} = I_{L_1} - I_{L_2} \tag{13}$$

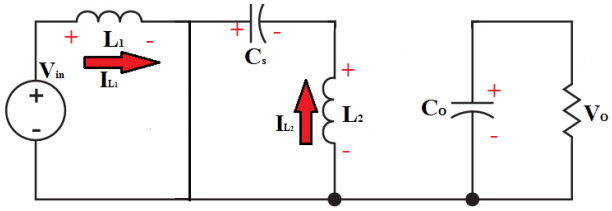

Fig. 5. Current Flow when Q_1 in OFF State

The switch is turns off after some time period and the current through inductor L_1 flows through the coupling capacitor and lastly, to the output capacitor and the load. When Q_1 is turned ON again, the capacitors get recharged and it delivers the load current and charge the inductor L_2.

3.2 Simulation of the SEPIC Converter

The converter is simulated using MATLAB/SIMULINK simulating environment and simulation parameters are listed in Table 4.

Table 4. Converter Parameter for Simulation

Specifications @ G =1000W/m^2	
Parameters	**Design Value**
Input Voltage, V_{in}	36V
Switching frequency, F_s	100kHz
Converter Output voltage, V_O	300V
Rated output power, P_O	80W
Inductors L_1 and L_2	2.4mH
Coupling capacitor, C_S	47µF
Output capacitor, C_O	10µF

The simulation model is derived as shown in Fig. 6 with the listed parameter in Table 4 and simulated using MATLAB/Simulink. The PWM pulse is generated by comparing the reference voltage and actual output voltage. In the feedback loop, a PI controller is employed and it is designed by loop shaping method.

The load voltage is sensed and fed to the comparator. To improve the steady and transient response of the converter, a PI controller is properly tuned using Ziegler-Nichols tuning method. The load with three different values are connected across the converter to check the effectiveness of the converter and the coefficients of a PI controller. The output voltage regulated by using a PI controller in the inner control loop.

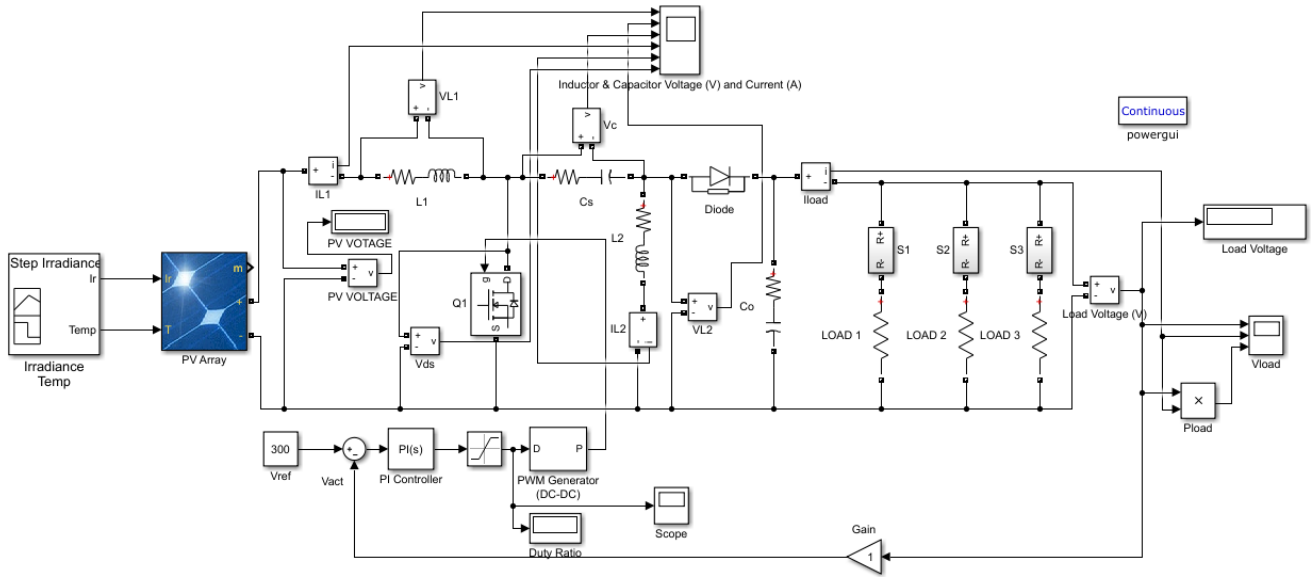

Fig. 6. Simulation Model of the SEPIC Converter

IV. Results And Discussions

As per the previous discussion, the converter is simulated with 60 cell PV array, the load with three different rating using MATLAB/Simulink simulation tool. The hardware prototype is developed with the specification listed in Table 3 and discussed in further section.

4.1 Effect of Change in Irradiance on PV Module

The solar irradiation is not constant throughout the day. So, it is important to study the effect of a change in irradiation on the solar PV module. Since the study is on the change in irradiation, the temperature is kept constant. The effect is shown in Fig. 7. From the Fig. 7, it is concluded that the load voltage is increased with increase in solar irradiation. With the increase in solar irradiation, the net output power is increased due to the increase in load current. Whereas, the net output power is reduced with an increase in temperature due to the decrease in load current.

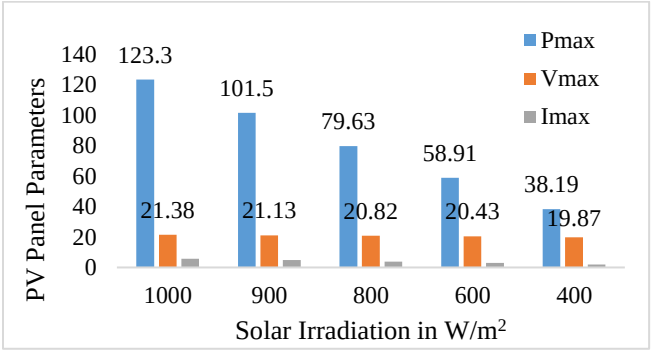

Fig. 7. Different Solar PV Parameters at 35ºC

4.2 Simulation Results

The load parameters and the SEPIC converter parameters are shown in Fig. 8 and Fig. 9 respectively. From the Fig. 8, it is seen that the converter took a finite time to reach the steady state. The results are verified for the two cases. In case-1, the control performance of the PI controller is tested by changing the solar irradiation from 1000W/m^2 to 800W/m^2 at 0.15 seconds and then to 600W/m^2 at 0.3 seconds and keeping load resistance constant at 100Ω. During both the changes, the load parameters are slightly oscillating and then reaches the steady state at the very fast rate. But the converter regulates the constant voltage even the solar irradiation changes up to 600W/m^2. Both the inductor voltages are equal in magnitude and opposite. The coupling capacitor blocks the DC current and the average inductor current is zero.

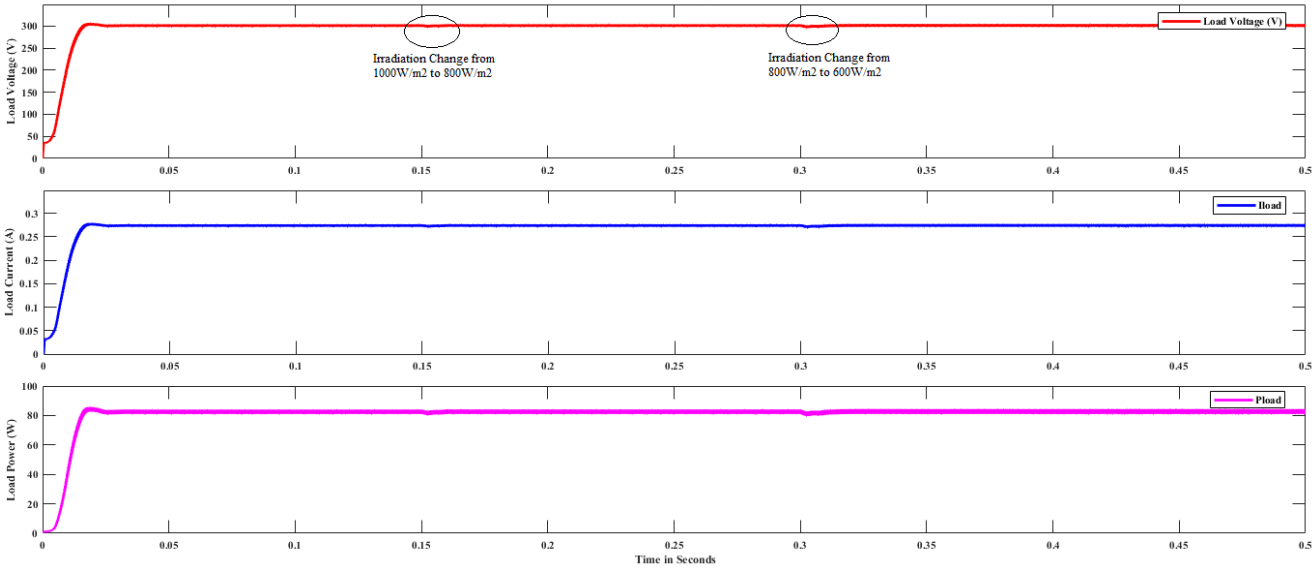

Fig. 8. Load Waveforms for Various Irradiation with Constant Load; (a) Load Voltage in Volt., (b) Load Current in Amp., (c) Output Power in Watt.

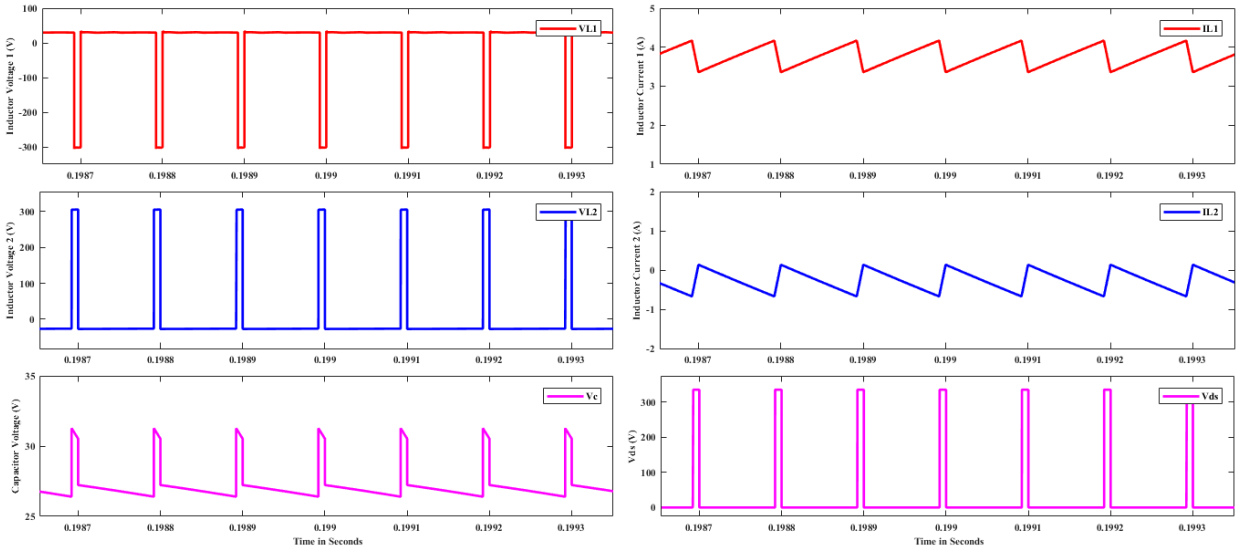

Fig. 9. Converter Waveforms for Various Irradiation with Constant Load; (a) Inductor (L_1) Voltage in Volt. & Inductor (L_1) Current in Amp., (b) Inductor (L_2) Voltage in Volt. & Inductor (L_2) Current in Amp., (c) Voltage across the Coupling Capacitor in Volt., (d) Switch Voltage in Volt

The load parameters and the SEPIC converter parameters are shown in Fig. 10 and Fig. 11 respectively. In case-2, the control performance of the PI controller is tested by changing the load resistance from 100Ω to 150Ω at 0.15 seconds and then to 200Ω at 0.3 seconds and keep the solar irradiation constant at 1000W/m^2. Similar to the previous case, the load parameters are slightly oscillating and then reaches the steady state at the very fast rate. The converter keep regulates the constant voltage even the load resistance changed from 100Ω to 200Ω. The load voltage is maintained constant and the load current is reduced as per the change in load resistance.

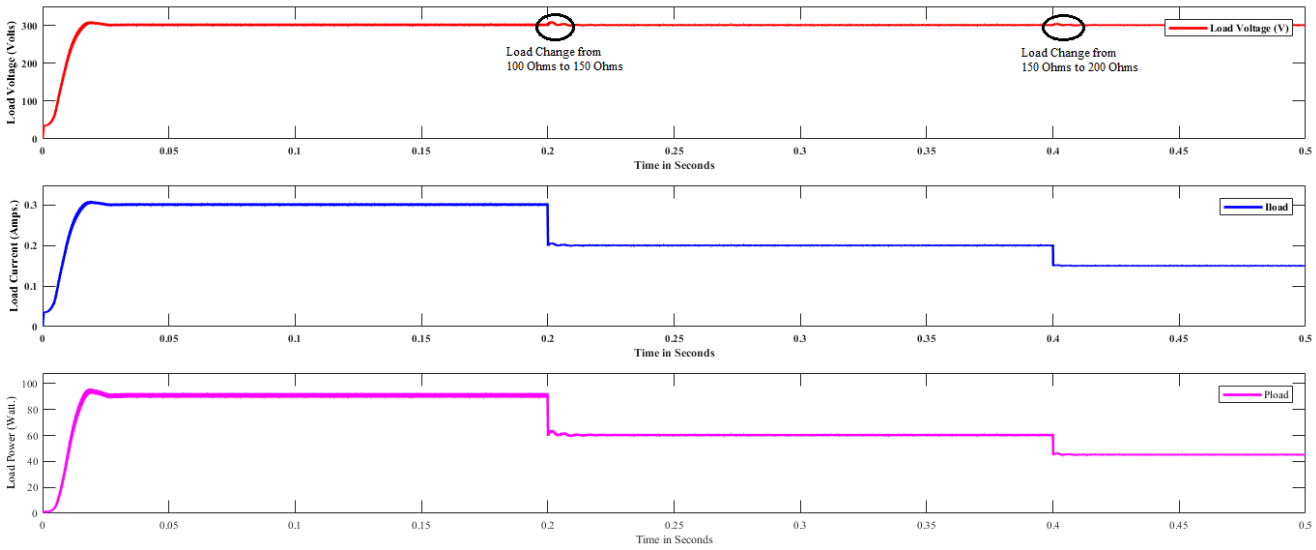

Fig. 10. Load Waveforms for Different Load with Constant Irradiation; (a) Load Voltage in Volt., (b) Load Current in Amp., (c) Output Power in Watt.

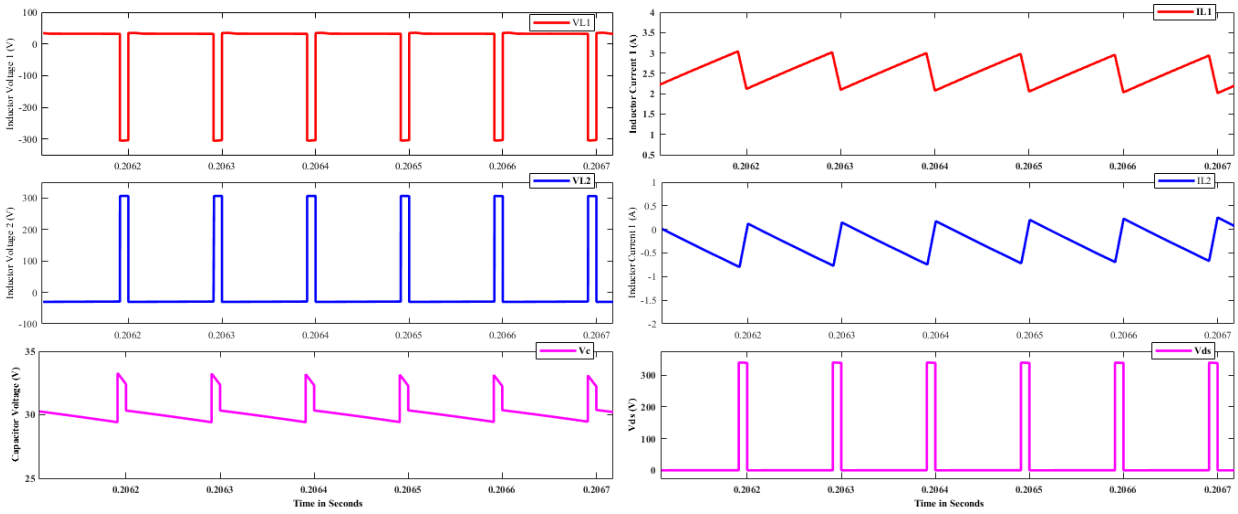

Fig. 11. Converter Waveforms for Various Irradiation with Constant Load; (a) Inductor (L_1) Voltage in Volt. & Inductor (L_1) Current in Amp., (b) Inductor (L_2) Voltage in Volt. & Inductor (L_2) Current in Amp., (c) Voltage across the Coupling Capacitor in Volt., (d) Switch Voltage in Volt

Before generating the gate pulse, the inductor ripple current need to be fixed at a certain value. If the allowed inductor ripple current is high, electromagnetic interference (EMI) will be increased. Whereas, if the current is low, there is a chance for unstable gating operation. So, it is better to fix the ripple current as 20-40% of the rated input current [10].

In this paper, the inductor ripple current selected as 30% of the rated input current.

4.3 Hardware Results

The following are the basic specification of the SEPIC converter. The various elements are selected as per the following value. The listed of components are given in Table 5.

Input voltage (V_{in}): 20 - 100V
Rated power (P_O) = 80W
Rated output voltage (V_O): 300 V
Rated output current (I_O): 0.3A
Switching frequency $(F)_s$: 10 kHz

Table 5. Various Components of the Converter

Elements	Type/Specifications
MOSFET	SiHF740
Diode, D	FR107
Capacitor, C_S	47µF, 100V (Ceramic)
Capacitor, C_O	10µF, 450V (Electrolytic)
Inductor L_1 & L_2	Powdered Iron Core, 2.4mH, 5A
D_{max} & D_{min}	92% & 82%

The windings of both the inductors are wound on the same core. The number windings of the two inductors are equal. The inductor ripple current splits equally to the two inductors due to the mutual inductance between the two windings. In practical, the inductance of both coils will not be same and it results in unequal ripple current through both the inductors. The experimental setup of the converter is shown in Fig. 12 and the converter performance is verified at 38ºC, 1000W/m^2 irradiation.

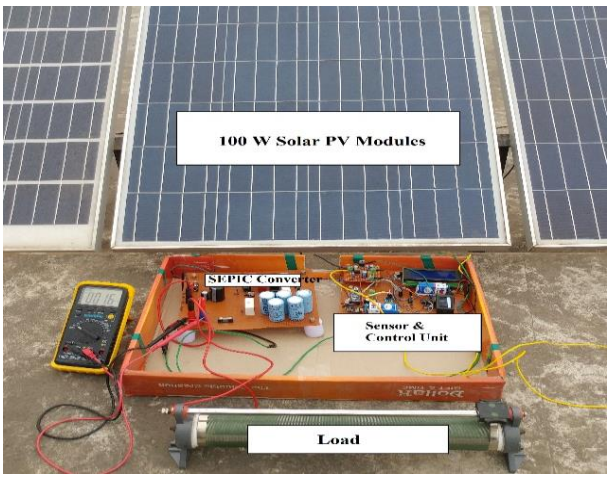

Fig. 12. Experimental Setup of Proposed Converter

From the observation, the PV output voltage is kept oscillating due to change in irradiation. However, the converter maintains the constant output voltage as per the desired output voltage. The converter rating is 80W at the normal operating condition. The load in this paper is considered as the resistive load. The output voltage is taken as a feedback with improved gain so that the PI controller reduce the error with respect to the actual output voltage. The hardware waveforms are shown in Fig. 13. Fig. 13(a) shows the gate-source voltage. The SiHF740 is driven through IR2113 MOSFET driver and it amplifies the gate-source voltage to 10V as shown in Fig. 13(a). The voltage across the coupling capacitor is shown in Fig. 13(b). The average voltage across this capacitor is 45V. The load voltage and the input voltage are shown in Fig. 13(c). The small oscillation in Fig. 13(c) indicates the instant at which change in load resistance.

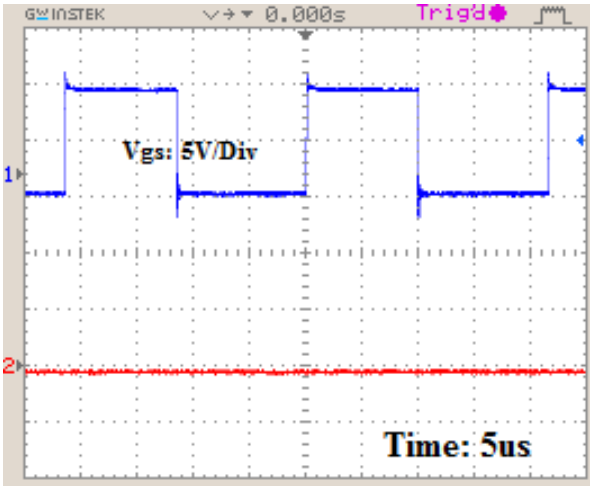

(a)

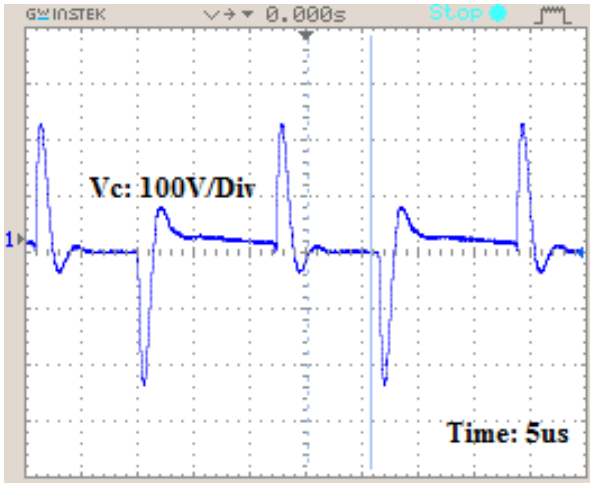

(b)

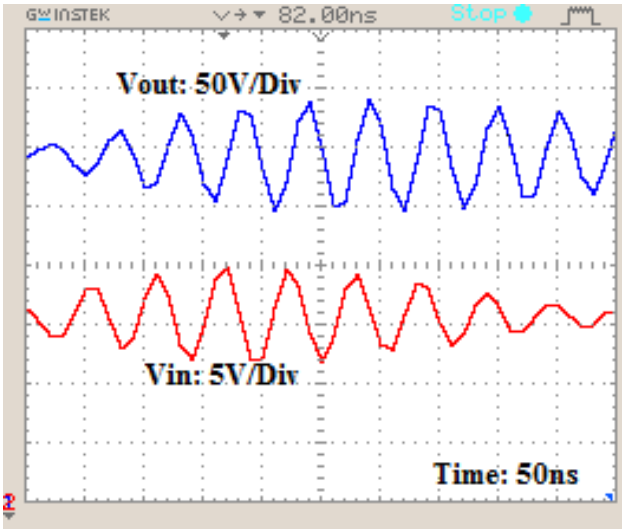

(c)

Fig. 13. Hardware Waveforms; (a) Gate-source Voltage in Volt., (b) Coupling Capacitor Voltage in Volt., (C) Input and Output Voltage in Volt.

The overall performance of the converter is shown in Table 6. The efficiency of the converter is assumed as 97%, drain-source current (I_{ds}) of the MOSFET is calculated as follows:

$$I_{ds} = {P_{in}}/{\eta V_{in}\sqrt{D}} = {80}/{0.97 * 40\sqrt{0.52}} = 2.86\ A \quad (14)$$

SiHF740 on-state resistance (R_{on}) is 0.05Ω and the resistance of the inductor (R_L) is 0.08Ω. So, the conduction loss of the MOSFET is estimated as follows:

$$P_{CL} = R_{on} * {I_{ds}}^2 = 0.408\ W \quad (15)$$

$$P_{Cu} = R_L * {I_{ds}}^2 = 0.65\ W \quad (16)$$

From the data sheet, the diode on-state voltage is taken as V_d=1.3V and conduction loss of the diode is calculated as follows:

$$I_{diode} = {P_o}/{V_o} = \frac{80}{385} = 0.207A \quad (17)$$

$$P_d = V_d * I_{diode} = (0.207) * (1.3) = 0.269W \quad (18)$$

From the datasheet of SiHF740, the discharged energy at C_{oss} is 1.5µJ. So, turn on loss is calculated as follows:

$$P_{on}^{Coss} = E_{C_{oss}} * Fs = 1.5\mu * 100 * 10^3 = 0.15W \quad (19)$$

The overlap loss is estimated in Eq. 20 and total on-time loss is given in Eq. 21. The turn off loss of the converter is presented in Eq. 22.

$$P_{on}^{Overlap} = \int_0^{t_{off}} I_{ds} * V_{ds} dt * Fsw = 0.1\mu * 100 * 10^3 * 2.86 * 95 = 0.271W \quad (20)$$

$$P_{on}^{total} = P_{on}^{C_{oss}} + P_{on}^{Overlap} = 0.421W \quad (21)$$

$$P_{off}^{Overlap} = \int_0^{t_{on}} I_{ds} * V_{ds} dt * Fsw = 0.04\mu * 100 * 10^3 * 2.86 * 95 = 1.08W \quad (22)$$

The total loss is given by equation 31 and efficiency of the converter is presented in equation 32.

$$P_{loss} = P_{on}^{total} + P_d + P_{off}^{Overlap} + P_{CL} + P_{Cu} = 2.83W \quad (23)$$

Table 6. Performance of the Converter

Type of the loss	Actual Loss
Switching loss	1.50W
Conduction loss (MOSFET and diode)	0.677W
Inductor losses	0.65W
MOSFET driver power consumption	0.24W
Controller power consumption	0.14W
Total Loss	3.208W
Efficiency at the rated power is 96.14%	

V. Conclusion

In this paper, the SEPIC converter is modelled, analyzed and implemented with the closed-loop control. The simulation results show that the solar PV power depends on environmental condition and the converter extracts the maximum power from the panel in both the cases of testing as discussed in section 4.2. Through the period of switching, the inductors maintain the constant voltage. The power rating of the converter less. So, it allows the designer to select the low on-state resistance SiHF740 MOSFET and it offers less switching loss. The converter is implemented with low-cost Arduino development board and it consumes low power. The reliability of the converter is high since the rating of the converter is less than 300W. The converter is rated for 80W so it is suitable for low power microconverter. The converter is implemented with DSP processor or FPGA development board, but in this paper, Arduino is used because the rating is below 100W.

References

[1] Baifeng Chen, Bin Gu, Lanhua Zhang, Zaka Ullah Zahid, Jih-Sheng Lai, Zhiling Liao, Ruixiang Hao: High-Efficiency MOSFET Transformerless Inverter for

Non-isolated Microinverter Applications. In: IEEE Transactions on Power Electronics, XXX (2015), No.7, July 2015, p.3610-3622.

[2] Dongbing Zhang: AN-1484 Designing A SEPIC Converter. In: Texas Instrument Application Report-SNVA168E, May 2006–Revised April 2013, p.3-42.

[3] David Meneses, Oscar Garcia, Pedro Alou, Jesus A. Oliver, Jose A. Cobos: Grid-Connected Forward Microinverter with Primary-Parallel Secondary-Series Transformer. In: IEEE Transactions on Power Electronics, XXX (2015), No.9, September 2015, p.4819-4830.

[4] Jason Tao, Vieri Xue: Grid-Connected Micro Solar Inverter Implement Using a C2000 MCU. In: Texas Instrument Application Report-SPRABT0, January 2013, p.3-28.

[5] Minjie Chen, Khurram K. Afridi, David J. Perreault: A Multilevel Energy Buffer and Voltage Modulator for Grid-Interfaced Microinverters. In: IEEE Transactions on Power Electronics, XXX (2015), No.3, March 2015, p. 1203-1219.

[6] M.Ramkumar, I.Sayed mohammed , J.Manikanda prashath: Simulation of SEPIC-CHMLI based Microinverter for High Step-up Voltage Conversion. In: International Journal of Innovative Research in Science, Engineering and Technology, III (2014), No.4, April 2014, p.10871-10880.

[7] M.Premkumar, N.Dhanasekar, R.Dhivakar, P.Arunkumar: Comparison of MPPT Algorithms for PV Systems based DC – DC Converter. In: Advances in Natural and Applied Sciences, XVII (2016), No.9, March 2016, p. 212-221.

[8] M.Premkumar, R.Jeevanantham, S.Muthu Vignesh kumar: Single Phase Module Integrated Converter Topology for Microgrid Network. In: International Journal of Innovative Research in Electrical, Electronics, Instrumentation and Control Engineering, II (2014), No.3, March 2014, p.1322-1325.

[9] P.I. Muoka, M.E. Haque, A. Gargoom, M. Negnevitsky: Modeling and Simulation of a SEPIC Converter based Photovoltaic System with Battery Energy Storage. In: Proceedings of 22nd Australasian Universities Power Engineering Conference, Bali, November 2012, p.1-6.

[10] Vuthchhay Eng, Unnat Pinsopon, Chanin Bunlaksananusorn: Modeling of a SEPIC Converter Operating in Continuous Conduction Mode. In: Proceedings of 6th International Conference on Electrical Engineering/Electronics, Computer, Telecommunications and Information Technology, Pattaya, Chonburi, 2009, p.136-139.

[11] Y. Jiang, Y. Wang, Q. Sun, Y. Wu: A Fault Prediction Method for Closed-Loop SEPIC Converters Under Variable Operating Conditions. In: Proceedings of Prognostics and System Health Management Conference, Chengdu, 2016, p.1-7.

[12] M. A. Al-Saffar, E. H. Ismail, A. J. Sabzali and A. A. Fardoun: An Improved Topology of SEPIC Converter with Reduced Output Voltage Ripple. In: IEEE Transactions on Power Electronics, XXIII (2008), No.5, September 2008, p.2377-2386.

[13] C. G. Bianchin, R. Gules, A. A. Badin, E. F. Ribeiro Romaneli: High-Power-Factor Rectifier Using the Modified SEPIC Converter Operating in Discontinuous Conduction Mode. In: IEEE Transactions on Power Electronics, XXX (2015), No.8, August 2015, p.4349-4364.

[14] H. Ma, Y. Li, J. S. Lai, C. Zheng, J. Xu: An Improved Bridgeless SEPIC Converter without Circulating Losses and Input Voltage Sensing. In: IEEE Journal of Emerging and Selected Topics in Power Electronics, Early Access, November 2017, p.1-10.

[15] R. Moradpour, H. Ardi and A. Tavakoli: Design and Implementation of a New SEPIC-Based High Step-Up DC/DC Converter for Renewable Energy Applications. In: IEEE Transactions on Industrial Electronics, LXV (2018), No.2, February 2018, p.1290-1297.

[16] Hu, Jingying, Anthony D. Sagneri, Juan M. Rivas, Yehui Han, Seth M. Davis, David J. Perreault: High-Frequency Resonant SEPIC Converter with Wide Input and Output Voltage Ranges. In: IEEE Trans. Power Electronics, XXVII (2012), No.1, January 2012, p.189–200.

[17] Dileep G, S. N. Singh, G. K. Singh: Modelling, Design and Stability Analysis of an Improved SEPIC Converter for Renewable Energy Systems. In: International Journal of Electronics, CIV (2017), No.9, 2017, p.1527-1545